IJoCED

Indonesian Journal of Computing, Engineering, and Design

Journal homepage: http://ojs.sampoernauniversity.ac.id/index.php/IJOCED

# Analyzing Fast-ions Trajectories in a Nuclear Fusion Reactor through Its Poincaré-Island Size and Ripple Resonance

*Anggi Budi Kurniawan[1*], Hiroaki Tsutsui[1]*

[1] Department of Transdisciplinary Science and Engineering, School of Environment and Society, Tokyo Institute of Technology, 2-12-1 Ookayama, Meguro-ku, Tokyo 152-8550, Japan

*Corresponding email: anggi@mers.nr.titech.ac.jp

**ABSTRACT**

Fast-ions confinement is a prominent subject in developing nuclear fusion reactors due to its importance in sustaining the burning plasma and keeping energy production. However, confining them has proven to be difficult until now, and one of the reasons is that the inherent discrete magnetic field produces a magnetic ripple. A better understanding of fast-ions transport using appropriate numerical calculation tools needs to be developed to overcome such a challenge in the engineering aspect. This study revisited data collection of fast ion transport simulated under the ripple presence in a nuclear fusion device. The ion trajectories were followed using two orbit-following equation schemes, and the ripple-resonance island size in the Poincaré section was compared. The result showed that the island size obtained by each scheme was different when the particle resonates with a stronger ripple field and, proportionally, the diffusion coefficients are different. The physical meaning and consequence behind this discovery were discussed in this paper.

**ARTICLE INFO**

*Article History:*
*Received 22 Feb 2021*
*Revised 09 Apr 2021*
*Accepted 04 Sept 2021*
*Available online 25 Sep 2021*

*Keywords:*
*Fast ion,*
*Full orbit,*
*Guiding center,*
*Magnetic resonance,*
*Precession island,*
*Tokamak.*

## 1. INTRODUCTION

Nuclear fusion is one of the most promising candidates for a large-scale clean energy source fuelled by light elements such as hydrogen isotopes. Countries worldwide are currently racing to create an artificial sun with fusion reaction and extract its massive energy, while some other developments are proposed for space exploration engines. The leading practical reactor candidate to harness its power is Tokamak, a doughnut-shaped device that utilizes a strong magnetic field to confine the plasma. Among many tokamak designs, spherical Tokamak (ST) is

currently on a high rise due to its compact design and low overall cost with weaker magnetic field operation (Harrison, 2019). In the future, this could potentially be a competitor for its counterpart, nuclear fission reactor, within similar compactness such as Indonesia's upcoming experimental power reactor (Reaktor Daya Eksperimental, RDE). However, our existing technology and knowledge still face many challenges in every engineering aspect. Most nuclear fusion development projects worldwide revolve around the thermonuclear approach, which involves high density and very high-temperature plasma to ignite fusion. Sustaining such plasma for a long time with an excellent input-output energy balance is highly required, and one promising solution is to utilize fast ions produced by the fusion reaction itself.

One fusion reaction among other candidates at the upfront discussion for fusion experiment is the deuterium-deuterium reaction, D(d,p)T, better known as D-D fusion. It produces a 1 MeV fast triton which held some critical roles such as aiding the tritium breeder system and simulating alpha particle confinement properties in DT plasma (Ogawa et al., 2019; Onofrio, 2018; Reichert, 2019).

In order to utilize the fast ions correctly and efficiently, they must be well confined in the magnetic field. However, confining them has proven difficult due to the magnetic ripple existence, which causes an abrupt ripple-induced diffusion phenomenon, raising particle loss fraction (McClements, 2005; Mcclements et al., 2018; Tobita et al., 1997). Such problem is rooted from energy-dependence ripple resonance (Hosseininejad, Ghoranneviss, & Salem, 2020; Hideyuki Mimata et al., 2009), but the complete process of particle loss remains unclear until now. It is then necessary to have a better understanding of fast ions transport with numerical study so that we can engineer a great confinement system in the future.

Numerical studies of fast ion trajectory have long been instrumented by two governing equations, guiding center (GC) and full orbit (FO) (Boozer, 1980; K. Tani et al., 2009; Keiji Tani, Azumi, Kishimoto, & Tamura, 1981). There is no comprehensive study that tells how different is the performance of both schemes at the moment, but one study suggested that the resonance energies by GC scheme are somewhat different from those by the FO scheme despite using a relatively strong magnetic field environment (Kurniawan, Tsutsui, Tani, & Shinohara, 2020; H. Mimata et al., 2008). However, the difference of resonance island and its consequence to ripple-resonance diffusion was not carefully studied and creates a knowledge gap for the future study on global fast-ion confinement using an appropriate tool. Hence, this study was conducted in the scope of local transport to add an understanding of global transport. The physical difference of ripple resonance island between both equation schemes in estimating fast triton's ripple resonance diffusion was investigated, and the general engineering point of view was discussed.

The remainder of this paper is organized as follows. Section 2 explains the numerical modelling used in this study, including a brief explanation of the interesting point for the triton's ripple resonance condition given the initial condition. In section 3, the precession island size difference in Poincaré mapping in the framework of result difference between FO and GC schemes was discussed, then the diffusion coefficient profile was briefly discussed following the respective island size. Finally, section 4 remarks the closing of this paper with the conclusion and future work.

## 2. RESEARCH METHODOLOGY

### 2.1. Plasma Parameter

This study uses plasma parameters of JT-60SA tokamak with operation scenario #3. It is selected by the fact that it can be used to conduct experimental studies related to particle confinement using fast triton (JT-60SA Research Unit, 2018). Moreover, there were not many studies involving this operation scenario (Garzotti et al., 2018) and therefore the present study is conducted with scenario #3 to also add the understanding of it.

### 2.2. Simulation Tool

Fortran-based orbit following Monte Carlo code OFMC is utilized and performed in a supercomputer system. OFMC modeling capabilities have been tested and verified both numerically and experimentally (Hirayama, Shimizu, Tani, Shirai, & Kikuchi, 1988; ITER Physics Expert Group & ITER Physics Basis Editors, 1999; Tobita et al., 1997).

### 2.3. Orbit-Following Schemes

Both guiding center and full orbit equations schemes are used in this study. The GC scheme has been well defined in some papers (Goldston, White, & Boozer, 1981; López, Orozco, Dugar-Zhabon, & Cardenas, 2019), and the FO scheme is based on the paper by Tani et al. (2009).

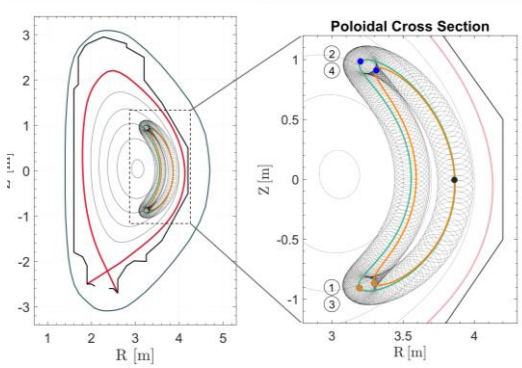


**Figure 1. Banana orbit of 1 MeV triton, moving in a clockwise direction on the poloidal cross-section**

Representation of both schemes is shown in **Figure 1**, which shows the collisionless banana trajectory of 1 MeV triton after orbiting for several bounces. GC scheme generates the orange line trajectory, while the FO scheme generates particle orbit (black, gyrating line) and the gyrocenter line (green). From this point onwards, all results from GC are plotted with orange color, and FO are plotted in green color. The present study focuses on the upper banana tip location. It must be noted that the result from the FO scheme should be considered as a reference for the GC scheme and not in reverse because FO represents the real particle trajectory motion.

### 2.4. Test Particle Condition

A moderately-trapped fast triton is simulated and launched at the outer midplane ($\boldsymbol{Z_0}$ = 0.0 m) of poloidal cross-section in ($\boldsymbol{R}, \boldsymbol{Z}, \boldsymbol{\phi}$) coordinate system from two major radial positions, $\boldsymbol{R_0}$ = 3.7 m and $\boldsymbol{R_0}$ = 3.86 m, with initial pitch angle $\boldsymbol{\gamma_0}$ = 70°. In the Poincaré map analysis, those values are referred to as "reference starting point." These conditions are selected based on the study by Kurniawan et al. (2020), which guarantees the observation of resonance condition without having the particle loss to either plasma center or outside of separatrix (i.e., orange line in **Figure 1**). The analysis was primarily conducted on collisionless orbit cases. The collision case, i.e., neoclassical diffusion, is briefly shown in the discussion section to investigate the consequence of having the island size difference on the collisionless discussion.

### 2.5. Poincaré Mapping

The particle orbit is reflected at a certain location as previously shown in **Figure 1**, thus leaving its banana tip trace in velocity space with each successive bounce point that can be visualized using Poincaré plot.

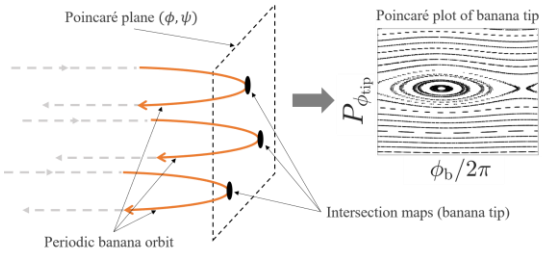


**Figure 2. Illustration of particle orbit bounces periodically (left), leaving the velocity trace at tip positions such as canonical angular momentum P_ϕ and can be visualized in a Poincaré map (right)**

In the particle study, it is important to discover the resonance condition using Poincaré plot before proceeding to much more complex analysis in a non-ideal MHD system (White, Gorelenkov, Duarte, & Berk, 2018). In this study, the velocity space is measured by toroidal canonical angular momentum $\boldsymbol{P_\phi = mRv_\phi - e\psi}$ on Poincaré section $(\boldsymbol{\phi, P_\phi})$. Definition of canonical angular momentum has been described in some papers (Hideyuki Mimata et al., 2009; K. Tani, Takizuka, & Azumi, 1993; Yushmanov, 1990). Each successive bounce points can be marked in a Poincaré map as illustrated in **Figure 2** and each bouncing point can be expressed as follows (White et al., 1996):

$$\psi_i^+ = \psi_i^- + \Delta_b \sin\left(N\phi_i^- + \frac{\phi}{4}\right) \quad (1)$$

$$\phi_i^+ = \phi_i^- + \phi_b(\psi_i^+) + \phi_p(\psi_i^+) \quad (2)$$

$$\psi_{i+1}^- = \psi_i^+ + \Delta_b \sin\left(N\phi_i^+ - \frac{\phi}{4}\right) \quad (3)$$

$$\phi_{i+1}^- = \phi_i^+ - \phi_b(\psi_{i+1}^-) + \phi_p(\psi_{i+1}^-) \quad (4)$$

The open surface (straight line) on the map indicates non-resonance phase, while the closed surface (island) indicates resonance. As mentioned in the previous subsection, the initial calculation is in the reference starting point whose Poincaré surface always in the middle of Poincaré map. Then, the map is scanned with an interval of 0.01 m/surface to obtain the Poincaré surfaces surrounding the reference point. After the Poincaré map obtained, the range value of canonical angular momentum $\boldsymbol{P_{\phi-tip}}$ (ordinate) and normalized toroidal angle $\boldsymbol{\phi_{bN}}$ (abscissa) on each banana tips' Poincaré surface will be measured and visualized in a graph. The range value will be discussed through the difference between maximum and minimum value, denoted as $\boldsymbol{\Delta P_{\phi-tip}}$ and $\boldsymbol{\Delta\phi_{bN}}$, and measured in arbitrary units.

## 2.6. Ripple Resonance Energy

The interest point of this study lies in the banana orbit that bounces in or near the ripple well region, allowing the expansion of resonance islands around banana tip and ease the observation. The term "weaker field" is used for the condition of where the ripple well $\delta$ is stronger, with a relationship of $B \propto 1/\delta$.

According to Yushmanov (1990), banana particles resonate with toroidal ripple when they satisfy the following condition,

$$\Delta\phi_p = \frac{2\pi}{N} \times k \quad (5)$$

where $N$ is the number of toroidal field coils, $k$ is positive/negative integer value, and $\Delta\phi_p$ is the toroidal angle difference between two successive precession orbit tips ($\boldsymbol{\Delta\phi_p = \phi_{p,i} \pm \phi_{p,i+1}}$). Based on the previous study, the corresponding value of $\Delta\phi_p$ depends on the particle energy as a function of gyro radius and hence proportionally affects the banana tip position. The ripple-resonance energies being investigated in this study correspond to $k$ = 2, which are considered as nearby to 1 MeV energy, and are shown in **Table 1**.

**Table 1. Ripple Resonance Energies**

| $R_0$ [m] | Scheme | $E_{r,k=2}$ [MeV] |
|---|---|---|
| **3.70** | GC | 0.88 |
| | FO | 0.76 |
| **3.86** | GC | 1.12 |
| | FO | 0.93 |

## 3. RESULTS AND DISCUSSION

### 3.1. Near-resonance Precession Island

Prior discussing the precession island at resonance energies, the result of 1 MeV triton is observed beforehand. The 1 MeV triton in this study is considered a near-resonance condition due to its proximity with ripple resonance energy given in **Table 1**.

**Figure 3** shows the Poincaré surface size of 1 MeV banana triton tip with two reference starting points, $\boldsymbol{R_0}$ = 3.7 m and $\boldsymbol{R_0}$ = 3.86 m. Left figures are measured by $\boldsymbol{\Delta P_{\phi-tip} = P_{\phi-max} - P_{\phi-min}}$ on each surface while the right figures are measured by $\boldsymbol{\Delta \phi_{bN} = (\phi_{b-max} - \phi_{b-min})/2\pi}$. The abscissa $\mathcal{N}$ represents the integer of the observed surface section where higher $\mathcal{N}$ value resides on the upper part of Poincaré section and indicates the outer side of minor radial position (i.e., plasma radius). The black dots on the figures indicate the surface of the tips launched from the reference starting point. The result indicates a different Poincaré surface between GC and FO schemes when the particle energy is fixed (in this case, 1 MeV).

**Figure 3 (a)** indicates the Poincaré map of FO scheme has a well-developed open surface and hence the arbitrary size is almost conserved, indicating the precession motion of 1 MeV tritons does not match the field repetition harmonics; it does not ripple resonance all over the observed surface. On the other hand, the GC scheme somewhat shows the precession island between $\mathcal{N}$= 16 and $\mathcal{N}$ = 20 which is about to satisfy the condition in Eq. (5). In **Figure 3 (b)**, the island size between FO and GC is quite similar in $\boldsymbol{\Delta P_{\phi-tip}}$ but not in $\boldsymbol{\Delta \phi_{bN}}$. Note that the scale of $\boldsymbol{\Delta P_{\phi-tip}}$ for $\boldsymbol{R_0}$ = 3.86 m is larger than that of $\boldsymbol{R_0}$ = 3.7 m. This is understandable because the magnetic field is relatively weaker at a higher radial position.

Based on the finding in **Figure 3** where some island is formed, combining with analytical estimation by Mimata et al. (2009) regarding the continuous representation of ripple-resonance island (p. 4-5), a Poincaré map with a well-developed resonance island is expected to have a sharp M-shape curve on $\boldsymbol{\Delta P_{\phi-tip}}$ graph and a sharp valley on $\boldsymbol{\Delta \phi_{bN}}$ graph. The more the number of $\mathcal{N}$ inside the M-shape (i.e., shaded area on the graph), the better the resonance island is developed. To verify the situation, further explanation of resonance precession island is discussed in the next subsection.

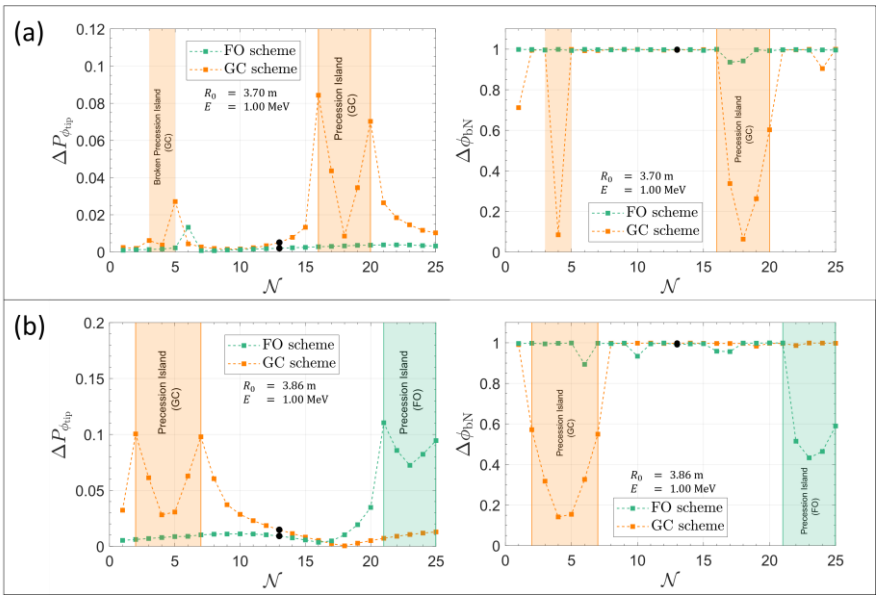


**Figure 3. Poincaré map and its surface's arbitrary size for 1 MeV triton banana tips on the flux surface with local ripple field, launched from the reference starting point, (a) $R_0$ = 3.7 m and (b) $R_0$ = 3.86 m**

Complementing the information to the study by Kurniawan et al. (2020), the radial positions of the island are different if the particle energy is fixed as indicated by **Figure 3 (b)**. It shows that the resonance island obtained by the FO scheme is located at the outer plasma radius relative to the island of GC scheme. In a real tokamak machine, the change of magnetic field is sensitive in the radial direction that it can change the resonance condition with just a slight radial move, while orbit precession in toroidal direction $\boldsymbol{\phi}$ dictates ripple resonance condition of a banana particle at the same time according to Eq. (5). Hence, the ripple resonance condition highly depends on the initial condition of the test particle.

### 3.2. Resonance Precession Island

Since the resonance energies are different between GC and FO schemes when the initial radial position is fixed as shown in **Table 1**, the Poincaré maps of both schemes are presumably similar in the ripple resonance case. **Figure 4** shows the Poincaré surface size of banana triton tips with resonance energies. Each surface is measured the same way as the previous subsection.

Ripple-resonance energies by GC and FO schemes were previously known to be slightly different when the initial position is fixed. On the other hand, the banana tip positions, which dictate the ripple-resonance condition, are different when the energy is fixed. Such conditions may affect the precession island size, particularly when the ripple resonance condition is stronger (i.e., in a weaker field). The precession island curve in velocity space $P_\phi$ obtained by GC scheme in a weaker magnetic field region (i.e., larger ripple well region at $R_0$ = 3.86 m) is different from FO scheme.

**Figure 4 (a)** indicates that the Poincaré maps of both FO and GC schemes agree to each other at $\boldsymbol{R_0}$ = 3.7 m, as well having a similar well-developed island size despite located in a very slightly different Poincaré surface $\boldsymbol{\mathcal{N}}$. Since this location has a stronger field, the $\boldsymbol{\Delta P_{\phi-tip}}$ of the precession island is quite small. It is understandable since the tritons have ripple resonance energy to begin with. **Figure 4 (b)** shows a rather agreeable in terms of precession island location between FO and GC schemes, but the island size in velocity space is somewhat different. All curves in Figure 4 show that sharp M-shape $\boldsymbol{\Delta P_\phi}$ curves and sharp $\boldsymbol{\Delta\phi_{bN}}$ valleys are developed in both FO and GC schemes with more $\boldsymbol{\mathcal{N}}$ inside of it, indicating well-developed resonance islands. Different island sizes can cause a different result; hence it is important to emphasize which orbit following scheme is appropriate to be utilized under the condition given in the study of particle transport.

It is notable in **Figure 4 (b)** that the island size difference measured on $\boldsymbol{\Delta P_{\phi-tip}}$ between FO and GC schemes are noticeable, with GC scheme has almost 3 times the size of that from FO scheme. It indicates that more banana particle tips are estimated to be trapped inside the island of GC scheme than FO scheme upon orbiting.

This difference is caused by a different ripple amplitude being experienced by the triton tips when calculated by FO and GC schemes. Magnetic field change is sensitive in a radial direction. GC scheme has its banana tip located on the outer radial position than FO scheme (see **Figure 1**). Hence, the triton in GC scheme experienced a weaker field, allowing a larger resonance island expansion around the banana tip. The result of **Figure 4 (b)** is an important finding in the present study.

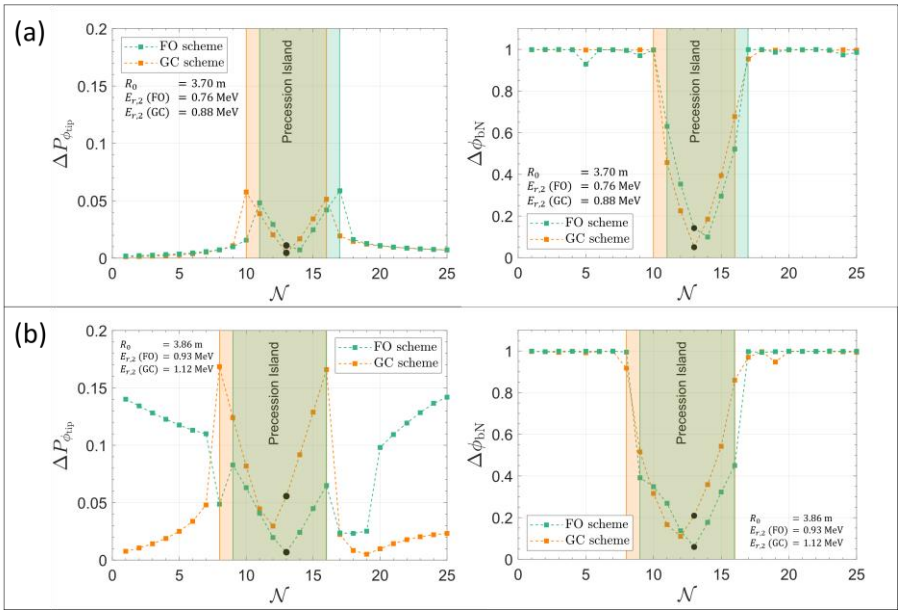


**Figure 4. Poincaré map and its surface's arbitrary size for triton banana tips with ripple-resonance energies on the flux surface with local ripple field, launched from the reference starting point, (a) $R_0$ = 3.7 m and (b) $R_0$ = 3.86 m**

**Table 2. Precession Island Size Difference Between FO and GC Schemes**

| $R_0$ [m] | Scheme | $E$ [MeV] | $\Delta P_{\phi-tip}$ | $\Delta \phi_{bN}$ |
|---|---|---|---|---|
| **3.70** | GC (res.) | 0.88 | 0.058 | 0.996 |
| | FO (res.) | 0.76 | 0.058 | 0.998 |
| | GC | 1.00 | 0.084 | 0.817 |
| | FO | 1.00 | - | - |
| **3.86** | GC (res.) | 1.12 | 0.168 | 0.918 |
| | FO (res.) | 0.93 | 0.082 | 0.654 |
| | GC | 1.00 | 0.100 | 0.572 |
| | FO | 1.00 | 0.109 | 0.791 |

As previously mentioned, the more the number of Poincaré surface $\mathcal{N}$ inside the M-shape curve, the better the resonance island is developed. However, it must be carefully understood that a well-developed island does not mean the local particle transport is better. It rather indicates more tritons are being disrupted during orbiting because more particle orbit tips are trapped inside the resonance island at a certain period and can cause a problem to the triton transport. Therefore, island size is an important parameter in estimating the local particle transport. The island size that we discuss so far is shown in **Table 2**. It is also important to note that the most important parameter is the $\Delta P_{\phi-tip}$, because it directly indicates the velocity space (canonical angular momentum) which was known to be strongly related to local ripple-resonance transport of particles.

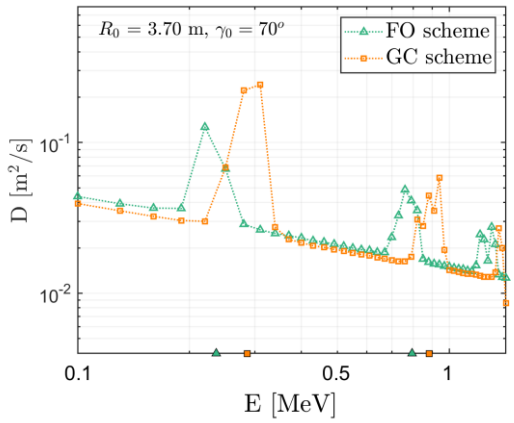


**Figure 5. Energy-dependence diffusion coefficient profile of triton launched at $R_0$ = 3.7 m and $\gamma_0$ = 70°**

### 3.3. Ripple-resonance Diffusion Profile

This subsection is presented to confirm the results on two previous subsections. The diffusion coefficient is evaluated from time-evolution ensemble canonical angular momentum with a relation of $D \equiv$

$d/dt\left(\langle\left(P_\phi - \langle P_\phi\rangle\right)^2\rangle/2\right)$, calculated by introducing Coulomb collision term $D \approx \Delta x^2/\Delta t$ into both FO and GC schemes. This evaluation method was first introduced by Tani et al. (1981). A swarm of 20000 fast tritons is collided with bulk plasma with electron density $n_e$ = 4.455 × $10^{19}$ $m^{-3}$ and temperature $T_e$ = 6.69 keV at our calculation point. Since the test particles are fast tritons, it is safe to assume that the collisionless orbit still plays a major part in determining the ensemble canonical angular momentum of those particles. Hence, **Figure 5** is presented to verify the consequence of having a result in **Figure 3 (a)**. In the case of **Figure 4 (a)**, it is not discussed further since it shows a good agreement between FO and GC schemes.

**Figure 5** shows the local diffusion coefficient profile of fast tritons launched from the midplane $R_0$ = 3.7 m. It presents the ripple-enhanced diffusion profile around ripple resonance energy level. When the ripple resonance condition is stronger due to weaker magnetic field, a good M-shaped coefficient profile around resonance energy level will be developed as reported by Mimata et al. (2009). However, since the ripple amplitude in our observation point is smaller, the M-shape is rather dull. Nonetheless, it still indicates a ripple resonance condition. In this study, we call this M-shape a ripple resonance spectrum. Note that it should not be confused between the M-shape diffusion coefficient and the M-shape curve in $\Delta P_{\phi-tip}$ discussion, although they are related to each other.

**Figure 3 (a)** has shown us that the GC scheme develops a resonance island while the FO scheme does not. It can be easily confirmed upon comparing with **Figure 5** because the 1 MeV triton is expected by GC scheme to be still around the ripple resonance spectrum. In the perspective of slowing down particle, it means that the 1 MeV tritons are about to enter ripple resonance condition and hence the resonance island in Poincaré map occurred. The same thing does not happen to the FO scheme, in which 1 MeV tritons are far from the ripple-resonance spectrum, giving it a non-resonance condition, and hence no precession island has occurred.

Next, the result of **Figure 3 (b)** and **Figure 4 (b)** are compared with the calculation result by Kurniawan et al. (2020), in which they discuss the diffusion coefficient for 10000 bulk tritons with a similar initial condition and launched at the midplane (p. 5). In the case of 1 MeV particle, it is found that FO and GC have a similar diffusion coefficient magnitude despite being located in a different spectrum. It is located on the right side of ripple-resonance spectrum in FO scheme, but in the GC scheme it is located on the left side. In the slowing-down particle perspective, a 1 MeV particle in FO scheme is about to enter ripple resonance while GC scheme predicts that it leaves the resonance condition. Hence, the precession island size of FO and GC schemes in **Figure 3 (b)** are identical despite having a different situation.

Kurniawan et al. (2020) also found that the M-shape diffusion coefficient is well developed in GC scheme ($E_{r,gc}$ = 1.116 MeV) but duller in FO scheme ($E_{r,fo}$ = 0.929 MeV). In the case of **Figure 4 (b)**, the resonance island of FO scheme is about 3 times smaller than GC scheme. It means the triton is predicted by FO scheme to experience a smaller ripple amplitude than that by GC scheme. Consequently, the ripple-resonance spectrum by FO scheme has a rather dull M-shape. These analyses are consistent with a previous study about the effect of ripple amplitude on the diffusion coefficient (Hideyuki Mimata, Tsutsui, Tsuji-Iio, Shimada, & Tani, 2008). Such difference can be interpreted in a way that the GC scheme estimates more banana tips trapped inside the resonance island. Hence

largely expanding the island and estimating a more abrupted diffusion coefficient that occurs around ripple-resonance energy (i.e., sharper ripple-resonance spectrum). On the other hand, FO scheme estimates rather fewer banana tips being trapped in the resonance island, giving what is considered as a less abrupted local ripple-induced diffusion process. In addition, the difference gives a strong indication that the weaker the magnetic field is, the difference between FO and GC schemes is larger.

Based on the findings in this section, a further study is needed to explore more about what makes the result between FO and GC schemes different. For example, one can approach a free parameter of particle characteristics inside either FO or GC scheme that does not possess by another. Theoretically, it affects the canonical angular momentum $P_\phi$ obtained by both schemes and the analytical expression may be given. To solve the different results, it is then necessary to conduct a future study to find the analytical difference between FO and GC schemes. Theoretically, we can simply use it to compensate the result from GC approximation so that it can produce a closer result with FO scheme. Such analysis is important to deepen our understanding and to efficiently use an appropriate numerical tool when studying the particles' global confinement from an engineering perspective. A different estimation on diffusion coefficient will potentially affect the accuracy of future numerical experiments, which may raise a questionable result that will affect the engineering design of magnetic field systems in the future development phase of nuclear fusion reactor like Tokamak.

From the computational point of view, it will be much more efficient than, for example, developing the guiding center in higher order, because it will not require a complex code update or larger resource to perform. This is especially true since guiding center equation is more popular for studying particle behavior because of its capability to approximate the particle drifting motion in a strong magnetic field. GC approximation is also resource-friendly which is considered timesaving and has lower CPU power consumption, but its accuracy will eventually break when we conduct a study in a weaker magnetic field (e.g., in MAST or STEP). Keep in mind that today's computer performance has been growing rapidly, so it is advised to use only the full orbit equation for further energetic particle studies based on our findings. However, they should be the study scope for future study and for that, we give our final remarks in the next section based on the present results.

## 4. CONCLUSION

Investigation of fast-ion trajectories through the difference of resonance precession island in Poincaré section between the guiding center (GC) and full orbit (FO) orbit-following schemes was performed. The $\Delta P_{\phi-tip}$ curve of GC scheme has a sharper M-shape than that of FO scheme, suggesting the banana tips were trapped more in the inner side of the magnetic ripple island on Poincaré map. Hence, a different estimation of particles' local transport between both schemes is expected. Such situations must be carefully considered when studying a particle transport and trajectory in a Tokamak nuclear fusion reactor, especially those with a weaker field like spherical tokamak. For that, the finding of this study will be used as the basis of our future work about a comprehensive analysis of GC-FO scheme difference in estimating the ripple-resonance transport of fast ions where we will develop further analytical expression.

The finding in this study is considered for the development of, but not limited to, tokamak fusion devices. Such ripple-

resonance phenomena may arise in other systems with magnetic field variation along the line such as cyclotron, by which Indonesia has a plan to build them for medical radionuclides production. On the other hand, if Indonesia decides to have a nuclear fusion device in the future, ripple-resonance diffusion phenomena must be carefully considered because it can affect the device's confinement performance and judge the overall capital cost.

**ACKNOWLEDGEMENT**

This work was supported by the National Institutes for Quantum and Radiological Science and Technology (QST, Japan). The authors would like to appreciate Dr. Keiji Tani and Prof. K. Shinohara for their advice and support on this work.

**REFERENCES**

Boozer, A. H. (1980). Guiding center drift equations. *Physics of Fluids*, *23*(5), 904–908. https://doi.org/10.1063/1.863080

Garzotti, L., Barbato, E., Garcia, J., Hayashi, N., Voitsekhovitch, I., Giruzzi, G., … Zagórski, R. (2018). Analysis of JT-60SA operational scenarios. *Nuclear Fusion*, *58*(2). https://doi.org/10.1088/1741-4326/aa9e15

Goldston, R. J., White, R. B., & Boozer, A. H. (1981). Confinement of high-energy trapped particles in Tokamaks. *Physical Review Letters*, *47*(9), 647–649. https://doi.org/10.1103/PhysRevLett.47.647

Harrison, R. (2019). Overview of new MAST physics in anticipation of first results from MAST Upgrade. *Nuclear Fusion*, *59*, 112011. https://doi.org/10.1088/1741-4326/ab121c

Hirayama, T., Shimizu, K., Tani, K., Shirai, H., & Kikuchi, M. (1988). *Experimental transport analysis code system in JT-60*. Retrieved from http://inis.iaea.org/search/search.aspx?orig_q=RN:19089954

Hosseininejad, M., Ghoranneviss, M., & Salem, M. K. (2020). Ripple transport and neoclassical diffusion in IR-T1 tokamak. *Journal of Theoretical and Applied Physics*, *14*(1), 93–99. https://doi.org/10.1007/s40094-019-00352-6

ITER Physics Expert Group, & ITER Physics Basis Editors. (1999). Chapter 5: Physics of energetic ions. *Nuclear Fusion*, *39*(12), 2471–2495.

JT-60SA Research Unit. (2018). *JT-60SA Research Plan*. Retrieved from http://www.jt60sa.org/pdfs/JT-60SA_Res_Plan.pdf

Kurniawan, A. B., Tsutsui, H., Tani, K., & Shinohara, K. (2020). Estimating ripple transport of moderately-confined fast tritons by D-D fusion in JT-60SA tokamak. *Plasma and Fusion Research*, *15*(2403057), 1–6. https://doi.org/10.1585/pfr.15.2403057

López, J. E., Orozco, E. A., Dugar-Zhabon, V. D., & Cardenas, P. A. (2019). López_2019_J._Phys.__Conf._Ser._1386_012128.pdf. *Journal of Physics: Conference Series*, *1386*, 012128. https://doi.org/10.1088/1742-6596/1386/1/012128

McClements, K. G. (2005). Full orbit computations of ripple-induced fusion α -particle losses from burning tokamak plasmas. *Physics of Plasmas*, *12*(7), 1–8.

https://doi.org/10.1063/1.1936532

Mcclements, K. G., Tani, K., Akers, R. J., Liu, Y. Q., Shinohara, K., & Tsutsui, H. (2018). confinement and neutron emission in the Mega The effects of resonant magnetic perturbations and charge-exchange reactions on fast ion con fi nement and neutron emission in the Mega Amp Spherical Tokamak. *Plasma Physics and Controlled Fusion*, *60*(095005). https://doi.org/10.1088/1361-6587/aad252

Mimata, H., Tani, K., Tobita, K., Tsutsui, H., Tsuji-Iio, S., & Shimada, R. (2008). Finite Larmor radius effects on ripple diffusion in tokamaks. *Progress in Nuclear Energy*, *50*(2–6), 638–642. https://doi.org/10.1016/j.pnucene.2007.11.071

Mimata, Hideyuki, Tani, K., Tsutsui, H., Tobita, K., Tsuji-Iio, S., & Shimada, R. (2009). Numerical study of the ripple resonance diffusion of alpha particles in tokamaks. *Plasma and Fusion Research: Regular Articles*, *4*(008).

Mimata, Hideyuki, Tsutsui, H., Tsuji-Iio, S., Shimada, R., & Tani, K. (2008). A theoretical model of ripple resonance diffusion of alpha particles. *Proceedings of ITC18*, *P1*(35), 261–264.

Ogawa, K., Isobe, M., Nishitani, T., Murakami, S., Seki, R., Nuga, H., … Osakabe, M. (2019). Energetic ion confinement studies using comprehensive neutron diagnostics in the Large Helical Device. *Nuclear Fusion*, *59*(7). https://doi.org/10.1088/1741-4326/ab14bc

Onofrio, R. (2018). Concepts for a Deuterium–Deuterium Fusion Reactor. *Journal of Experimental and Theoretical Physics*, *127*(5), 883–888. https://doi.org/10.1134/S1063776118110171

Reichert, S. (2019). Triton burn-up. *Nature Physics*, *15*(7), 622. https://doi.org/10.1038/s41567-019-0590-9

Tani, K., Nishio, S., Tobita, K., Tsutsui, H., Mimata, H., Tsuji-Iio, S., & Aoki, T. (2009). Ripple loss of alpha particles in a low-aspect ratio tokamak reactor. *IEEJ Transactions on Fundamentals and Materials*, *129*(9), 2004. https://doi.org/10.1541/ieejfms.129.569

Tani, K., Takizuka, T., & Azumi, M. (1993). Ripple loss of alpha particles in a tokamak reactor with a noncircular plasma cross-section. *Nuclear Fusion*, *33*(6), 903.

Tani, Keiji, Azumi, M., Kishimoto, H., & Tamura, S. (1981). Effect of Toroidal Field Ripple on Fast Ion Behavior in a Tokamak. *Journal of the Physical Society of Japan*, *50*(5), 1726–1737. https://doi.org/https://doi.org/10.1143/JPSJ.50.1726

Tobita, K., Tani, K., Kimura, H., Kusama, Y., Isobe, M., & Tobita, K. (1997). Loss of fast tritons in JT-6OU reversed magnetic shear discharges. *Nuclear Fusion*, *37*(1583).

White, R. B., Gorelenkov, N. N., Duarte, V. N., & Berk, H. L. (2018). Resonances between high energy particles and ideal magnetohydrodynamic modes in tokamaks. *Physics of Plasmas*, *25*(10), 102504. https://doi.org/10.1063/1.5046655

Yushmanov, P. N. (1990). Diffusive transport processes caused by ripple in tokamaks. *Review of Plasma Physics (Ed. B.B. Kadomtsev)*, *16*, 117–241.